Int J Adv Manuf Technol (2017) 90:3347–3355
DOI 10.1007/s00170-016-9605-1

ORIGINAL ARTICLE

Investigation on the influence of material crystallographic orientation on grinding force in the micro-grinding of single-crystal copper with single grit

Man Zhao[1] · **Xia Ji**[1] · **Beizhi Li**[1] · **Steven Y. Liang**[2]

Received: 16 June 2016 / Accepted: 10 October 2016 / Published online: 7 November 2016

Abstract In the micro-grinding process, owing to the size effect, the effects of material microstructure on the grinding force are more significant through the variation of material flow stress. Currently, the variation of material flow stress resulting from the change of crystallographic orientation during the micro-grinding has not been well examined. In this paper, a new predictive model for the variation of flow stress due to the process-induced change of crystallographic orientation is developed, which is based on the Taylor factor as determined by calculating the activated slip systems, thus quantifying the way crystallographic orientation affects both the number and the style of activated slip systems. Moreover, the predicted force is compared with previous reported experimental data on monocrystalline copper. As a result, the following findings are obtained from the comparison between the predicted result and the experimental data: (1) The predicted microgrinding force agrees well in trend with the experimental force, suggesting that the approach for predicting the grinding force based on the Taylor factor is feasible; (2) In the microgrinding of single-crystal materials, the feed rate direction relative to the crystallographic orientation has great effects on the flow stress and hence on the grinding force.

Keywords Microgrinding · Flow stress · Crystallographic orientation · Grinding force

✉ Xia Ji
jixia0206@163.com

[1] Donghua University, 2999 North Renmin Road, Songjiang district, Shanghai 201620, China

[2] Georgia Institute of Technology, 801 Ferst Drive, Atlanta, GA 30332, USA

Nomenclature

α_s	Effective rake angle
α_{cr}	Critical rake angle
α	Nominal rake angle
t	The depth of cut
r	The cutting edge radius
t_{cr}	The minimum undeformed chip thickness
k	A chip formation point on the grit edge
φ_k	Local shear angle
α_k	Local rake angle
θ_k	The angle between local shear force and the local total force
β_k	Local friction angle
T_0, T_m, T_w	Workpiece, ambient, and melting temperature
b	The local cutting width
$F_{tg,chip}$	Tangential chip formation force
A,B,C,m,n	Johnson–Cook parameters
$F_{ng,chip}$	Normal chip formation force
$F_{tg,plow}$	Tangential plowing force
$F_{ng,plow}$	Normal plowing force
F_S	Shear force on AB
F_N	Force normal to AB
F_C	Chip formation force
F_T	Thrust force
F	Friction force in boundary lubrication
R	Resultant force in boundary lubrication
N	Normal load in boundary lubrication
Γ_σ	Shear strain of all dislocation
M	Conventional Taylor factor
M^*	Verified Taylor factor
K_{cut}^{sp}	Cutting specific energy
HB	Brinell hardness
F_p	Indentation force

D	Grit diameter
σ	Total flow stress
σ_0	Thermally activated stress
σ_1	Athermal activation stress
ε	Plastic strain
ϵ_w	Effective strain
$\dot{\varepsilon}$	Plastic strain rate
M_1^*	Total Taylor factor
τ_s	Shear strength
$\dot{\varepsilon}_0$	Material constant
α_1	Constant
b_1	Burger vector
ρ_1	Density of dislocation
l	The length of the shear plane
V_s	Shear velocity
F_t, F_n	Total single grit force in the tangential and normal directions
v	Poisson's ratio
ρ	Density
K	Thermal conductivity
C_P	Specific heat
a_w	Cutting width
V	Cutting speed
Φ	Angle between the normal direction of slip plain and grinding plain in grain
Ω	Angle between slip direction and grinding direction in grain

1 Introduction

In recent years, an increase in the demands for micro components is shown in various industries. Mechanical micromachining is one of the best fabrication methods that create micro parts with complex dimensional features [1–4]. During these processes, the microgrinding is typically the final process step and it has a competitive edge compared with other fabrication processes. Besides, the microgrinding process is defined as the grinding with the ratio of the depth of cut [5] to the grit radius smaller than 1. Therefore material microstructure, grit edge radius, and undeformed chip thickness are in the same order of magnitude.

In conventional grinding process, grinding force is analyzed from three components—chip formation, plowing, and sliding. The sliding force is caused by the elastic or elastic–plastic contact of grit wear flat area with the workpiece surface [6]. Experimental investigations proved that the grinding force varies with different wear area [7]. In micro-grinding, the single interaction between the grit and a workpiece is more important because the microgrinding process is the cumulative outputs of numerous single-grit interactions. In this study, the micro grinding process shares the individual grit interaction model with microcutting in terms of the high negative angle and high strain rates, only considering both microcutting and plowing mechanisms along with associated friction effects at the contact interface [5].

In the microgrinding process, due to the size effect, the influences of material microstructure on the grinding force are more significant through the variation of material flow stress. The grinding force relates not only to the geometry of grain and material mechanical properties but also to the wheel surface topography. In this work, only the change in forces due to workpiece material anisotropy is considered since the other effects are already studied and can be included to the model afterwards [8–10].

Crystallographic orientation (CO), along with the grain size and grain boundary, has significant effect on the grinding force, temperature, and the part's quality. It was proved by Wu et al. [11] that crystallographic orientation had an important impact on the grinding force and the burr formation. Specifically, making the dislocation movement direction obliquely upward in front of the grinding direction was conducive to the reduction of the grinding force and the burr formation. Patten et al. [12] carried out the experiments on single-crystal silicon carbide and reported the variations of the forces due to the changes in CO. Sharif et al. [13] conducted experiments using the single-crystal synthetic diamond tool with different CO on its rake face, while the workpiece material was single-crystal silicon. The cutting and thrust forces showed the variations with respect to the tool's different CO and the surface finish of the workpiece was affected by the CO as well. Furthermore, Lee et al. [14] and Zhou et al. [15] reported the variation of surface roughness with the change in the CO caused by the diamond turning of the single-crystal copper. The crystallographic nature of the grinding force variation was also analyzed based on a microplastic model, and the analytical results revealed that the shear strength of a crystal was not constant for a given material but varied with the crystal orientation.

Basically, the above mentioned investigations [11–15] have qualitatively analyzed the effect of CO on the machining process, whereas a quantitative model has not been developed. At the same time, in the prediction of the flow stress, the Taylor factor affected by CO is developed as a fixed value [5, 16–20]. Consequently, the relationship between CO and grinding force has not been identified accurately, thus it is significant to develop a model to investigate the effect of CO on grinding force. Demir [21] presents a Taylor factor model to predict the forces and the cutting specific energy. This model is potentially applicable to the calibration of milling force models.

In this paper, a new predictive model for the variation of flow stress due to the process-induced change of crystallographic orientation is developed. Taylor factor, connected with the CO and shear angle, is determined by calculating the activated slip systems. In a mechanistic computation, the Taylor factor contributes to the flow stress that influences the grinding force, which also incorporates the prominent plowing effect in the microgrinding cases.

2 Mechanical physical modeling and calculation

2.1 Modeling the single grit interaction in micro-grinding

The micro-grinding process shares the individual grit interaction model with microcutting in the terms of the high negative angle and high strain rates, by considering the microchips as a series of elements with infinitesimal width, and it is also hypothesized that there is no heat loss along the primary and secondary heat zones, based on the assumption that there is no coolant in microgrinding [22].

2.1.1 Prediction of chip formation force

In this investigation, the abrasive grit shape on the wheel surface is assumed to be a spherical shape. Based on the assumptions, a mathematical framework for the individual grit interaction in the micro-grinding is started by assuming that the two-dimensional processes involve the microcutting and plowing phenomena, as shown in Fig. 1.

In micromachining, there are three important rake angles: (i) a negative rake angle (α_s) that changes according to the varying depth of cut; (ii) a critical rake angle (α_{cr}), which is the transition point from the microcutting and plowing; and (iii) the nominal rake angle (α).

The effective rake angle (α_s) is negative in the case where the undeformed chip thickness is smaller than the cutting edge radius. The instantaneous rake angle is obtained from a geometrical relationship as follows:

$$\alpha_s = \sin^{-1}\left(\frac{t-r}{r}\right) \tag{1}$$

where t is the depth of cut and r is the cutting edge radius.

The critical rake angle can be determined by the minimum undeformed chip thickness and the cutting edge radius according to following equation:

$$\alpha_{cr} = \sin^{-1}\left(\frac{t_{cr}-r}{r}\right) \tag{2}$$

where t_{cr} is the minimum undeformed chip thickness.

It should be noted that all the rake angles here have negative values. When the undeformed chip thickness t is larger than t_{cr}, the material removal mechanism is the chip formation and this microcutting mechanism can be represented by applying the Merchant model [23] to each of the infinitesimal elements. The incremental chip formation force can be expressed as

$$\begin{cases} dF_{tg,chip} = \dfrac{\tau_s \cos(\beta_k - \alpha_k)}{\sin\varphi_k \cos(\varphi_k + \beta_k - \alpha_k)} dt_{1k} \\ dF_{ng,chip} = \dfrac{\tau_s \cos(\beta_k - \alpha_k)}{\sin\varphi_k \cos(\varphi_k + \beta_k - \alpha_k)} dt_{1k} \end{cases} \tag{3}$$

where k represents a chip formation point on the grit edge, and the shear angle (φ_k) also changes with the infinitesimal rake angle (α_k) and can be got from the Oxley model [26]. Besides, τ_s is the shear stress, b is the local cutting width, and β_k is the local friction angle, which can be achieved from Eq. (4)

$$\beta_k = \theta_k + \alpha_k - \varphi_k \tag{4}$$

where θ_k is the angle between the local shear force and the local total force. The geometrical relationship between the angles is provided in Fig. 2.

From the geometrical relationship, the unit depth of cut can be expressed as follows:

$$dt_{1k} = r\cos\alpha_k d\alpha_k \tag{5}$$

The local width of the cut for each individual grit can be expressed as follows:

$$b = 2r\cos\alpha_k \tag{6}$$

Through the integration of the incremental tangential and normal forces per unit width in the two-dimensional

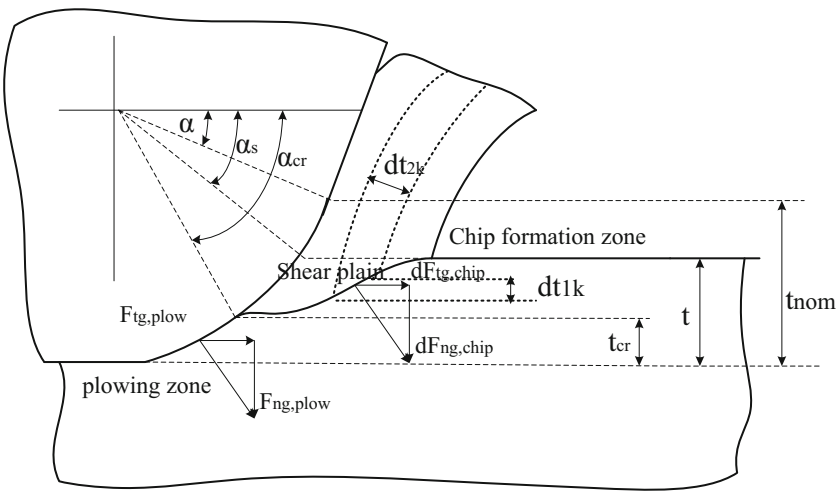

Fig. 1 Single grit interaction illustration

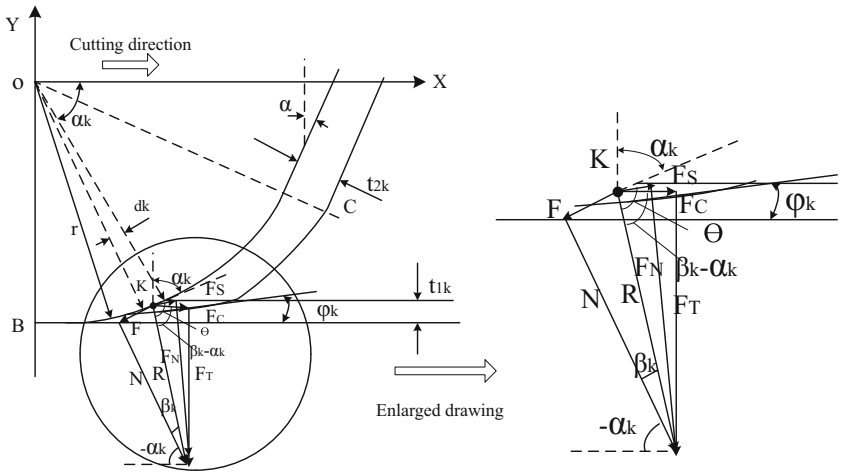

Fig. 2 Geometrical model for cutting force

simplified configuration, the chip formation force of each grit can be calculated. Then the total tangential and normal force can be expressed as

When $t < t_{\text{nom}}$,

$$\begin{cases} F_{\text{tg,chip}} = \int_{\alpha_{\text{cr}}}^{\sin^{-1}\frac{(t-r)}{r}} \dfrac{\tau_s \cos(\beta_k - \alpha_k)}{\sin\varphi_k \cos(\varphi_k + \beta_k - \alpha_k)} 2r^2 \cos^2\alpha_k d\alpha_k \\ F_{\text{ng,chip}} = \int_{\alpha_{\text{cr}}}^{\sin^{-1}\frac{(t-r)}{r}} \dfrac{\tau_s \sin(\beta_k - \alpha_k)}{\sin\varphi_k \cos(\varphi_k + \beta_k - \alpha_k)} 2r^2 \cos^2\alpha_k d\alpha_k \end{cases} \tag{7}$$

When $t > t_{\text{nom}}$,

$$\begin{cases} F_{\text{tg,chip}} = \int_{\alpha_{\text{cr}}}^{\alpha} \dfrac{\tau_s \cos(\beta_k - \alpha_k)}{\sin\varphi_k \cos(\varphi_k + \beta_k - \alpha_k)} 2r^2 \cos^2\alpha_k d\alpha_k \\ \qquad + \dfrac{\tau_s \cos(\beta - \alpha)(t - r(1 + \sin\alpha))r}{\sin\varphi \cos(\varphi + \beta - \alpha)} \\ F_{\text{ng,chip}} = \int_{\alpha_{\text{cr}}}^{\alpha} \dfrac{\tau_s \sin(\beta_k - \alpha_k)}{\sin\varphi_k \cos(\varphi_k + \beta_k - \alpha_k)} 2r^2 \cos^2\alpha_k d\alpha_k \\ \qquad + \dfrac{\tau_s \sin(\beta - \alpha)(t - r(1 + \sin\alpha))r}{\sin\varphi \cos(\varphi + \beta - \alpha)} \end{cases} \tag{8}$$

The terms $\varphi, \beta, and\ \alpha$ in Eq. (8) represent the nominal values of shear, friction, and rake angles, respectively.

$$\tau_s = \frac{\sigma^*}{\sqrt{3}} \tag{9}$$

2.1.2 Prediction of plowing force

In the Brinell test, the spherical tip is pressed against the workpiece surface, in which the plastic deformation zone similar to the stresses at the rounded tool and the workpiece interface in Fig. 3 is created. The Brinell hardness number (HB) is defined as the ratio of the load (F_p) to the curved area of the indentation as follows:

$$\text{HB} = \frac{F_p}{\pi D t_{\text{cr}}} \tag{10}$$

where D is the ball diameter, and t_{cr} is the critical undeformed chip thickness. In this analysis, the indentation force acting in the direction of α_{cr} with respect to the normal direction is attributed to the plowing force and friction between the grit and the workpiece is also generated by the relative movement.

The tangential and normal plowing forces per grit can be estimated by combining the indentation effect with the friction reaction as follows:

$$\begin{aligned} F_{\text{tg,plow}} &= F_p(\cos\alpha - u_p \sin\alpha) \\ F_{\text{ng,plow}} &= F_p(\sin\alpha + u_p \cos\alpha) \end{aligned} \tag{11}$$

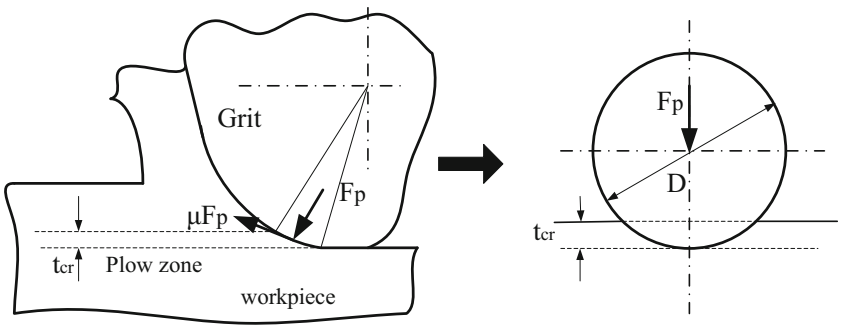

Fig. 3 Simplification of the plowing effects into a spherical indentation [5]

where u_p is the plowing friction coefficient, and $u_p = \tan\beta$.

The total single grit force in the tangential and normal directions is the sum of the forces caused by chip formation and plowing, namely:

$$\begin{aligned} F_t &= F_{tg,chip} + F_{tg,plow} \\ F_n &= F_{ng,chip} + F_{ng,plow} \end{aligned} \tag{12}$$

2.1.3 Flow stress model of single-crystal material

Flow stress can be divided into thermally activated stress and athermal stress based on the dislocation theory [24], which is given by

$$\sigma = \sigma_0 + \sigma_1 \tag{13}$$

where the thermally activated stress σ_0 represents the flow stress with a dislocation density of zero. In order to integrate the effect of temperature, strain, and strain rate, the Johnson–Cook model is adopted to represent the material deformation behavior on the shear plane, which is given by [25]

$$\sigma_0 = (A + B\varepsilon^n)\left(1 + C\ln\frac{\dot{\varepsilon}}{\dot{\varepsilon}_0}\right)\left(1-\left(\frac{T_0-T_w}{T_m-T_w}\right)^m\right) \tag{14}$$

The strain and strain–rate computations used in this work are based on Oxley [26] and the strain along the shear plane (tool-chip interface) is given by

$$\varepsilon = \frac{1}{2\sqrt{3}}\frac{\cos\alpha_k}{\sin\varphi_k\cos(\varphi_k-\alpha_k)} \tag{15}$$

The strain rate along the tool-chip interface is given by

$$\dot{\varepsilon} = \frac{1}{\sqrt{3}}\left(C\frac{V_s}{l}\right) \tag{16}$$

where C is a constant, l is the length of the shear plane ($l = dt_{1k}/\sin\varphi_k$) and V_s is the shear velocity related to the cutting velocity (V) by following equation:

$$V_s = V\frac{\cos\alpha_k}{\cos(\varphi_k-\alpha_k)} \tag{17}$$

The athermal activation stress model is proposed by Huges et al. [16] to represent the effect of dislocations as follows:

$$\sigma_1^* = M_1^*\alpha_1 G b_1\sqrt{\rho_1} \tag{18}$$

where M_1^* is the Taylor factor, α_1 is the material constant, G is the shear modulus of material, b_1 is the burger vector [16] of dislocations, and ρ_1 is the total density of dislocation. The modified material model of the microgrinding is proposed as follows:

$$\sigma^* = \sigma_0 + M_1^*\alpha_1 G b_1\sqrt{\rho_1} \tag{19}$$

2.2 Modeling of Taylor factor

2.2.1 The microplastic model

The physical theory of the Taylor factor has been developed and investigated based on the microplastic model [27].

The virtual work equation of single-crystal deformation can be formulated by [27]:

$$\sigma \mathrm{d}\epsilon_w = \tau_c d\Gamma_\sigma \tag{20}$$

where $d\Gamma_\sigma$ is the shear strain of all dislocation, and τ_c is the critical shear stress of the activated slip system.

The effective strain $\mathrm{d}\epsilon_w$ is connected to the shear strain of all dislocation by Taylor factor M.

$$\frac{d\Gamma}{\mathrm{d}\epsilon_w} = M \tag{21}$$

Therefore, the relationship between the normal stress and shear strength can be expressed:

$$\sigma = M\tau_c \tag{22}$$

2.2.2 Proposed model of Taylor factor

Schmidt. E et al. [28] proposed the Schmidt factor to investigate the tensile yield stress in material tensile test. Based on the critical shear stress formula $\tau_c = (F/A)\cos\Phi\cos\Omega$, the tensile yield stress can be formulated as

$$\sigma_s = m_c\tau_c \tag{23}$$

where $m_c = 1/(\cos\Phi\cos\Omega)$ is the reciprocal of Schmidt factor of slip system with the most orientation advantageous in grain and m_c varies with the change of polycrystalline crystallographic orientation. In the investigation, crystallographic orientation is presented by Miller's indices [29]. For example, [h k l] is parallel to the grinding direction, while [u v w] is perpendicular to the grinding direction.

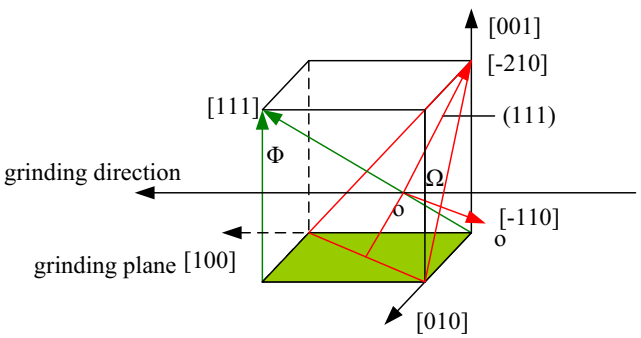

Fig. 4 Angles between the slip system direction and grinding direction

Table 1 The 12 slip systems of FCC crystal [11]

Plane	(111)			Plane	$(\bar{1}\bar{1}1)$		
Direction	$[01\bar{1}]$	$[\bar{1}10]$	$[0\bar{1}1]$	Direction	[011]	[101]	$[\bar{1}\bar{1}0]$
Plane	$(\bar{1}11)$			Plane	$(1\bar{1}1)$		
Direction	$[0\bar{1}1]$	$[\bar{1}0\bar{1}]$	[110]	Direction	[011]	$[10\bar{1}]$	$[\bar{1}\bar{1}0]$

In uniaxial drawing, the formula $M=m_c$ is built and the calculated value of m_c varies with different polycrystalline deformation models [30].

During the micro-grinding process, the plastic formation of the grinding chip is caused by the material dislocation slip. In one slip system, the sketch map is shown in Fig. 4, where Φ denotes the angle between the normal direction of the slip plane and the grinding plane in grain; Ω stands for the angle between the slip direction and the grinding direction in grain; and φ is the shear angle, which is assumed to be 10° in this paper. The formula of the verified Taylor factor can be express as follows:

$$M^{*} = {}^{1}\!/_{\cos(\Phi+\varphi)\cos(\Omega+\varphi)} \tag{24}$$

"Slip" refers to the movement of dislocations on certain crystallographic planes along certain crystallographic direction. The combination of slip plane and slip direction is called the "slip system", and each crystal system has a different number of slip systems. In the FCC crystals, the slip planes belong to the {111} family and the slip direction belongs to the <011> family. Considering the different unique planes and directions in these two families, it can be concluded that the FCC system has 12 slip systems and the 12 slip systems of FCC lattice are summarized in Table 1.

Therefore, the Taylor factor can be expressed as

$$M_1^{*} = \sum_{i=1}^{n} 1/(\cos(\Phi+\varphi)\cos(\Omega+\varphi)) \tag{25}$$

where, n refers to the total activated slip systems.

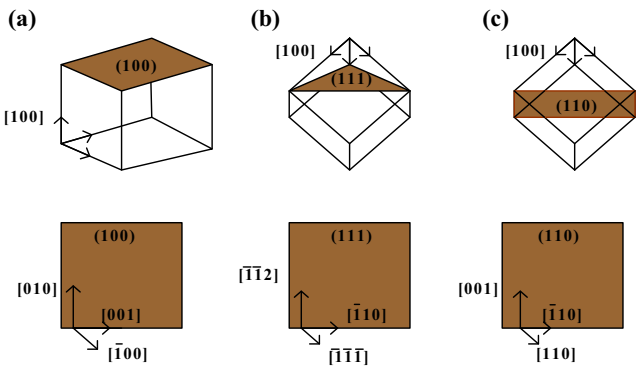

Fig. 5 Single-crystal copper workpieces. **a** <100>. **b** <111>. **c** <110> [11]

Table 2 Johnson–Cook parameters for materials and constants used in Eq. (19) [31]

Material	A (MPa)	B (MPa)	n	C	m	α_1	b_1 *(nm)*	ρ_1 *(nm^{-2})*
Copper	90	292	0.31	0.25	0.553	0.24	0.308	5×10^{-4}

2.2.3 Specific energy

Specific energy can be obtained in terms of the shear strength, the shear angle, and the hardness, as follows: [21]

$$K_{\mathrm{cut}}^{\mathrm{sp}} = \frac{M\tau_s}{\tan\varphi} - \frac{H}{3} \tag{26}$$

where τ_s is obtained from flow stress as shown in Eq.(9), and the flow stress is related to Taylor factor. However, it is different from the Demir's method [21], in which $\tau_s = M\tau_{cr}$, where τ_{cr} is the slip resistance.

2.3 Predicting cutting forces for oblique machining conditions

The main difference between oblique machining and orthogonal machining is that the chip flow direction is in general no longer normal to the cutting edge and the process is three-dimensional. The slope of the tool cutting face relative to the cutting velocity is one of the most important parameters in determining the cutting force. In oblique machining, it is not obvious which slope should be considered. Various equations which have been proposed for determining this direction are now considered. Lin and Oxley obtained equations for three components of cutting force F_C, F_T, and F_R in terms of normal plane values of shear angle [26]. The unit vector $\hat{c}$, $\hat{t}$, and $\hat{r}$ are along the three mutually perpendicular force component directions F_C, F_T, and F_R, respectively. So, the new Taylor factor can be included in the prediction model of cutting forces oblique machining conditions. Therefore, the resultant cutting force R in vector form is

$$R = F_C\hat{c} + F_T\hat{t} + F_R\hat{r} \tag{27}$$

The sense of both the side cutting edge angle C_s and the inclination angle i is to make the chip flow away from the axis of rotation of the work then P_1, P_2, and P_3 can be expressed as follows:

Table 3 Additional material properties used in the model [31]

Material	E (GPa)	v	H (Brinell)	ρ (kg/m^3)	K (W/m°C)	C_P (J/kg°C)	T_m (°C)
Copper	129.8	0.343	131	8960	399	386	1356

Table 4 Machining parameters of single-crystal copper [11]

The depth of cut	t (μm)	1.4, 3.5, 7, 10, 14
Cutting speed	v (m/min)	6
Cutting width	a_w (μm)	71.4
Cutting edge radius	r (μm)	5

Table 5 The Taylor factor of different grinding orientations

Cutting plane	(100)	(111)	(110)
Cutting direction	[001][010]	[$\bar{1}$10] [$\bar{1}\bar{1}$2]	[$\bar{1}$10] [001]
M_1^*	12.6834	61.3005	55.7638

$$\begin{aligned} P_1 &= F_C \\ P_2 &= F_T \cos C_s + F_R \sin C_s \\ P_2 &= F_T \sin C_s - F_R \cos C_s \end{aligned} \tag{28}$$

3 Model validation and discussion

3.1 Material parameter definition

Copper is a face-centered cubic (FCC) material. There are three single-crystal coppers (<100>, <111 > and <110>) that are tested with their crystal structures displayed in Fig. 5. In this figure, the upper surfaces are denoted by the crystal planes of (100), (110), and (111), which are perpendicular to the crystallographic orientation of <100>, <111>, and <110> in the crystal structure, respectively.

For the workpiece material, Johnson–Cook parameters of the material flow stress used for model validations are listed in Table 2 and additional material properties used to model forces are provided in Table 3.

3.2 Process parameter definition

The effects of undeformed chip thickness are investigated in the microcutting of single-crystal copper. Five undeformed chip thicknesses are considered, among which the undeformed chip thickness less and larger than as well as approximate to the cutting edge radius are selected. The cutting parameters are listed in Table 4.

3.3 Force prediction and comparison

The tangential and normal force under the given conditions can be predicted using Eq. (12) with the chip formation force and plowing force first computed using Eqs. (7), (8), and (10). Furthermore, the flow stress is computed using Eq. (19), and then τ_s is calculated using Eq. (9). The effects of strain, strain–rate, and temperature as well as CO are considered in the flow stress equation and the equivalent rake angle is calculated by the undeformed chip thickness as well as tool edge radius angle using Eq. (1). Then, the Taylor factor is obtained from Eq. (25). And the resultant value of the predicted Taylor factor is presented in Table 5:

The experimental data used in this work are obtained from Xian et al. [11].The comparison between the predicted grinding force and experimental grinding force is shown in Fig. 6, where FT is the tangential force and t is the depth of cut.

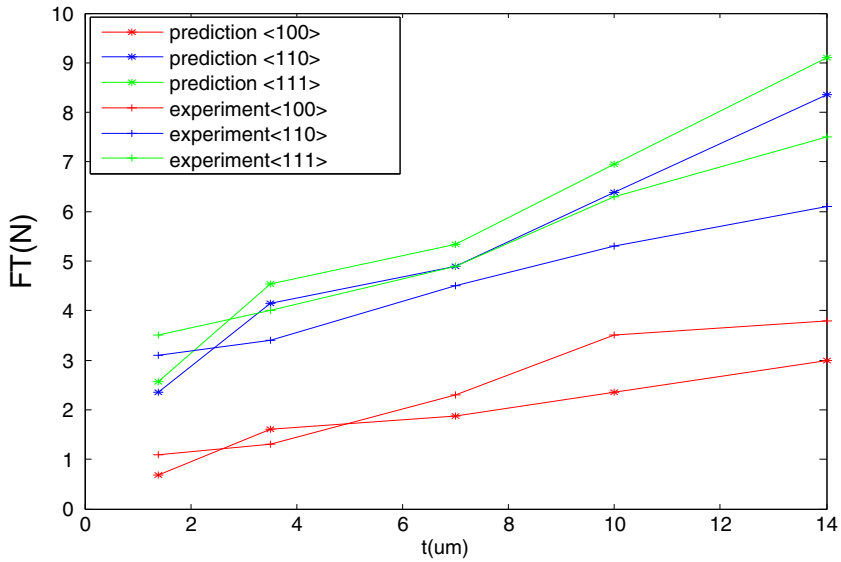

Fig. 6 The comparisons between prediction and simulation

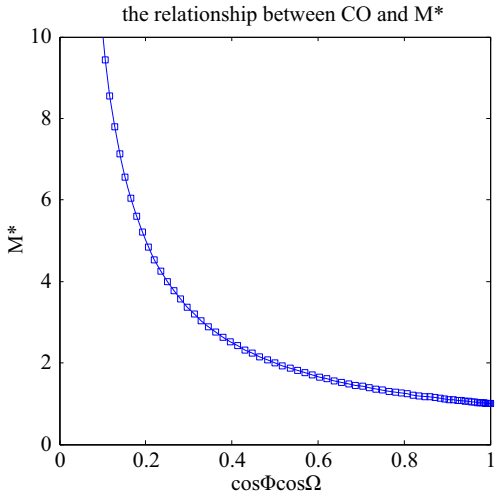

Fig. 7 The influence of crystal orientation on *M**

As the grit advances, the workpiece materials of the contact region between the grit and the workpiece slip along the slip planes with low Taylor factors. The comparison result shows that (1) the predicted micro-grinding force agrees well in trend with the experiment force, (2) the cutting force of the <111> workpiece is the maximum and that of <100> workpiece is the minimum both in experiment and prediction, and (3) Taylor factor has a significant effect on the cutting force. And it would be very useful to assess the effect on the specific energy [21]. The reasons for this deviation can be attributed to the determination of constants in the JC model, accurate determination of the tool edge radius as well as its change with the aggravation of the tool wear, the variation of dislocation density, and the estimation of process conditions such as friction.

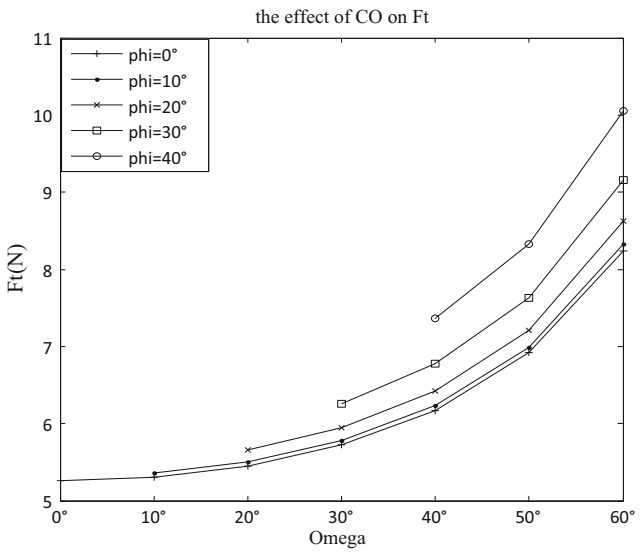

Fig. 8 The influence of crystal orientation on grinding force

3.4 Crystallographic orientation effect

3.4.1 Effect of crystallographic orientation on Taylor factor

Typically, the slip is restricted to a few of (symmetry-related) slip systems consisting of a slip plane and a slip direction, and it generally occurs when the local stress projected to the plane exceeds a critical value. Besides, the activation of one slip system depends on the cutting direction, and the initially activated slip system(s) may show single-slip or multi-slip activity. The plastic slip activity in the full model is defined as the sum of the absolute values of the plastic slip along all slip systems. If the resistance to this sliding is very high, the slip system with high *M** will not be activated. The relationship between the Schmidt factor and *M** is displayed in Fig. 7.

3.4.2 Effect of crystallographic orientation on grinding force

The effect of crystallographic orientation on grinding force is given as in Eq. (7–8). It is assumed that the value of Φ is fixed as $[0^\circ\, 10^\circ\, 20^\circ\, 30^\circ\, 40^\circ]$ and the corresponding Ω is Φ to 60°. The variation of grinding force is represented with the increase of Ω. and the variation of tangential force with crystallographic orientation is provided in Fig. 8.

It can be seen from Fig. 8 that the crystal orientations have an obvious effect on the micro tangential grinding force.

4 Conclusion

The micro-grinding process of monocrystalline copper has been investigated, with the emphasis put on the effects of crystallographic orientation on the chip formation force and plowing force. The predicted result and experiment data indicate that the tangential grinding force of the <111> workpiece and the <100> workpiece is respective the maximum and the minimum at the same depth of cut. Meanwhile, the predicted result matches well in trend with the experimental result when the crystallographic orientation is considered in the model, while the deviation between the experiment and prediction explains the dislocation density, which is variational in the machining process and regarded as a fixed value in the model.

The following conclusions are drawn from this study. In micro-grinding process, the Taylor factor has positive correlation with the variation of flow stress, and it plays a significant role in the grinding force. There are two elements that must be considered in the calculation of the Taylor factor: one is the number of the activated slip system and the other is the Schmidt factor of the activated slip system. In addition, the Schmidt factor in the paper is

calculated by considering not only the angles between the grinding direction and slip system but also the shear angle. Moreover, whether the slip system is activated or not depends on its Schmidt factor of grinding direction. In other words, a larger Schmidt factor makes it easier for the slip system to be activated.

Acknowledgements The authors would like to extend their thanks to the research project of state key laboratory of mechanical system and vibration MSV201604.

References

1. Chae J, Park SS, Freiheit T (2006) Investigation of micro-cutting operations. Int J Mach Tools Manuf 46(3–4):313–332
2. Chen MJ, Ni HB, Wang ZJ, Jiang Y (2012) Research on the modeling of burr formation process in micro-ball end milling operation on Ti–6Al–4V. Int J Adv Manuf Technol 62(9–12):901–912
3. Zhang T, Liu ZQ, Xu CH (2013) Influence of size effect on burr formation in micro grinding. Int J Adv Manuf Technol 68(9–12): 1911–1917
4. Zhan ZB, Li L, He N, Shrestha R (2014) An experimental study on grinding parameters for manufacturing PCD micro milling tool. Int J Adv Manuf Technol 73(9–12):1799–1806
5. Park HW (2008) Development of micro-grinding mechanics and machine tools, Dissertation, Georgia Institute of Technology
6. Malkin S (1989) Grinding technology: theory and applications of machining with abrasives. Ellis Howard Ltd, Prentice Hall
7. Li L, Fu J (1980) A study of grinding force mathematical model. Procedia CIRP 29:245–259
8. Meng P (2016) Microstructure and performance of monolayer brazed grinding wheel with polycrystalline diamond grains. Int J Adv Manuf Technol 83(1–4):441–447
9. Li HN, Yu TB, Zhu LD, Wang WS (2015) Modeling and simulation of grinding wheel by discrete element method and experimental validation. Int J Adv Manuf Technol 81(9–12):1921–1938
10. Li XK, Wolf S, Zhi G, Rong YM (2014) The modelling and experimental verification of the grinding wheel topographical properties based on the 'through-the-process' method. Int J Adv Manuf Technol 70(1–4):649–659
11. Wu X, Li L, He N, Zhao M, Zhan ZB (2015) Investigation on the influence of material microstructure on grinding force and bur formation in the micro grinding of copper. Int J Adv Manuf Technol 79(1–4):321–327
12. Patten J, Gao W, Yasuto K (2005) Ductile regime nanomachining of single-crystal silicon carbide. ASME J Manuf Sci Eng 127(3):522–532
13. Sharif UM, Seah KHW, Li XP, Rahman M, Liu K (2004) Effect of crystallographic orientation on wear of diamond tools for nanoscale ductile cutting of silicon. Wear 257(7–8):751–759
14. Lee WB, To S, Cheung CF (2000) Effect of crystallographic orientation in diamond turning of copper single crystals. Scr Mater 42(10):937–945
15. Zhou M, Ngoi BKA, Zhong ZW, Wang XJ (2001) The effect of material microstructure on micro-grinding processes. Mater Manuf Process 16(6):815–828
16. Hughes DA, Hansen N (2000) Microstructure and strength of nickel at large strains. Acta Mater 48(11):2985–3004
17. Hall EO (1951) The deformation and ageing of mild steel: III discussion of results. Proc Phys Soc B 64:747–753
18. Park HW, Liang SY (2008) Force modeling of micro-grinding incorporating crystallographic effects. Int J Mach Tools Manuf 48(15):1658–1667
19. Venkatachalam S, Fergani O, Li XP, Guo YJ, Chiang KN, Liang SY (2015) Microstructure effect on cutting force and flow stress in ultra-precision machining of polycrystalline brittle material. J Manuf Sci Eng 137(2):1–9
20. Venkatachalam S, Li XP, Fergani O, Guo YJ, Liang SY, Bryan MM (2013) Crystallographic effects on microscale machining of polycrystalline brittle materials. J Micro Nano-Manuf 1(4):1–11
21. Demir E (2008) A Taylor-based model for micro-machining of single crystal fcc materials including frictional effects-application to micro-milling process. Int J Mach Tools Manuf 48(14):1592–1598
22. Park HW, Liang SY (2009) Force modeling of microscale grinding process incorporating thermal effects. Int J Adv Manuf Technol 44(5–6):476–486
23. Merchant ME (1945) Mechanics of the metal cutting process. II plasticity conditions in orthogonal cutting J Appl Physics 16(6): 317–324
24. Abed FH, Voyiadjis GZ (2005) Plastic deformation modeling of AL-6XN stainless steel at low and high strain rates and temperatures using a combination of BCC and FCC mechanisms of metals. Mech Mater 37(8):1618–1639
25. Johnson GR, Cook WH (1985) A constitutive model and data for metals subject to large strain, high strain rates and high temperatures. Proceeding of the Seventh International Symposium on Ballistics, Hague, pp. 541–547
26. Oxley PLB (1989) The mechanics of machining: an analytical approach to assessing machinability. Ellis Horwood Limited, Chichester
27. Lee WB, Zhou M (1993) A theoretical-analysis of the effect of crystallographic orientation on chip formation in micromachining. Int J Mach Tools Manuf 33(3):439–447
28. Schimdt E, Boas W (1950) Plasticity of crystal. Springer and Hughes, Berlin and London
29. Ashcroft NW, Mermin ND (1976) The drude theory of metals. Solid State Physics, Harcourt, New York
30. Lin C (1999) China metallurgical encyclopedia, metal and plastic processing. metallurgical industry press, Beijing
31. Frutschy KJ, Clifton RJ (1998) High-temperature pressure-shear plate impact experiments on OFHC copper. J Mech Phys Solids 46(10):1723–1743